

Pre-training Everywhere: Parameter-Efficient Fine-Tuning for Medical Image Analysis via Target Parameter Pre-training^{*}

Xingliang Lei^{a,1}, Yiwen Ye^{a,1}, Zhisong Wang^a, Ziyang Chen^a, Minglei Shu^b, Weidong Cai^c, Yanning Zhang^a and Yong Xia^{a,*}

^aSchool of Computer Science and Engineering, Northwestern Polytechnical University, Xi'an, 710072, Shaanxi, China

^bShandong Artificial Intelligence Institute, Qilu University of Technology, Jinan, 250353, Shandong, China

^cSchool of Computer Science, The University of Sydney, Sydney, 2006, New South Wales, Australia

ARTICLE INFO

Keywords:

Medical image analysis,
Self-supervised learning,
Parameter-efficient fine-tuning

ABSTRACT

Parameter-efficient fine-tuning (PEFT) techniques have emerged to address overfitting and high computational costs associated with fully fine-tuning in self-supervised learning. Mainstream PEFT methods add a few trainable parameters while keeping the pre-trained backbone parameters fixed. These methods achieve comparative, and often superior, performance to fully fine-tuning, demonstrating the powerful representation ability of the pre-trained backbone. Despite this success, these methods typically ignore the initialization of the new parameters, often relying solely on random initialization. We argue that if pre-training is significantly beneficial, it should be applied to all parameters requiring representational capacity. Motivated by this, we propose Target Parameter Pre-training (TPP), a simple yet effective fine-tuning framework. TPP pre-trains target parameters, *i.e.*, the new parameters introduced during fine-tuning, in an additional stage before PEFT. During this stage, the pre-trained backbone parameters are frozen, and only the new parameters are trainable. A defined pretext task encourages the new parameters to learn specific representations of downstream data. Subsequently, when PEFT is employed, the pre-trained new parameters are loaded to enhance fine-tuning efficiency. The proposed TPP framework is versatile, allowing integration with various pre-trained backbones, pretext tasks, and PEFT methods. We evaluated the fine-tuning performance of our method on seven public datasets, covering four modalities and two task types. The results demonstrate that TPP can be easily integrated into existing PEFT methods, significantly improving performance.

1. Introduction

Deep learning has significantly advanced medical image analysis, markedly improving model performance Zhou, Siddiquee, Tajbakhsh and Liang (2019); Greenspan, Van Ginneken and Summers (2016). However, these models often require large-scale, high-quality annotated datasets, which are particularly time-consuming and labor-intensive to produce in medical imaging Dutt, Ericsson, Sanchez, Tsafaris and Hospedales (2024); Wu, Wu, Shi, Picker, Chong and Cai (2023). Consequently, medical image analysis frequently encounters challenges related to limited dataset sizes Willemink, Koszek, Hardell, Wu, Fleischmann, Harvey, Folio, Summers, Rubin and Lungren (2020), which hinders its clinical application. Self-supervised learning (SSL) has gained prominence due to its reduced data demands, high accuracy, and strong generalization ability. SSL typically involves two stages: pre-training on a large-scale unlabeled dataset and fine-tuning on labeled datasets. While various pretext tasks are employed for pre-training, SSL-pre-trained models Chen, Kornblith, Norouzi and Hinton (2020); Azizi, Mustafa, Ryan, Beaver, Freyberg, Deaton, Loh, Karthikesalingam, Kornblith, Chen et al. (2021); Kang, Song, Park, Yoo and Pereira (2023); Ye, Xie, Zhang, Chen, Wu and Xia (2024) are typically fully fine-tuned during the downstream task, updating all pre-trained parameters.

^{*}This work was supported by the National Natural Science Foundation of China under Grants 92470101.

^{*}Corresponding author.

✉ leixingliang@mail.nwpu.edu.cn (X. Lei); ywye@mail.nwpu.edu.cn (Y. Ye); zswang@mail.nwpu.edu.cn (Z. Wang); zychen@mail.nwpu.edu.cn (Z. Chen); shum1@sds.org (M. Shu); tom.cai@sydney.edu.au (W. Cai); ynzhang@nwpu.edu.cn (Y. Zhang); yxia@nwpu.edu.cn (Y. Xia)

ORCID(s): 0009-0003-6260-4061 (X. Lei); 0000-0003-2189-6865 (Y. Ye); 0009-0009-4764-3699 (Z. Wang); 0000-0002-8564-9735 (Z. Chen); 0000-0002-7136-1538 (M. Shu); 0000-0003-3706-8896 (W. Cai); 0000-0002-2977-8057 (Y. Zhang); 0000-0001-9273-2847 (Y. Xia)

¹These authors contributed equally to this work.

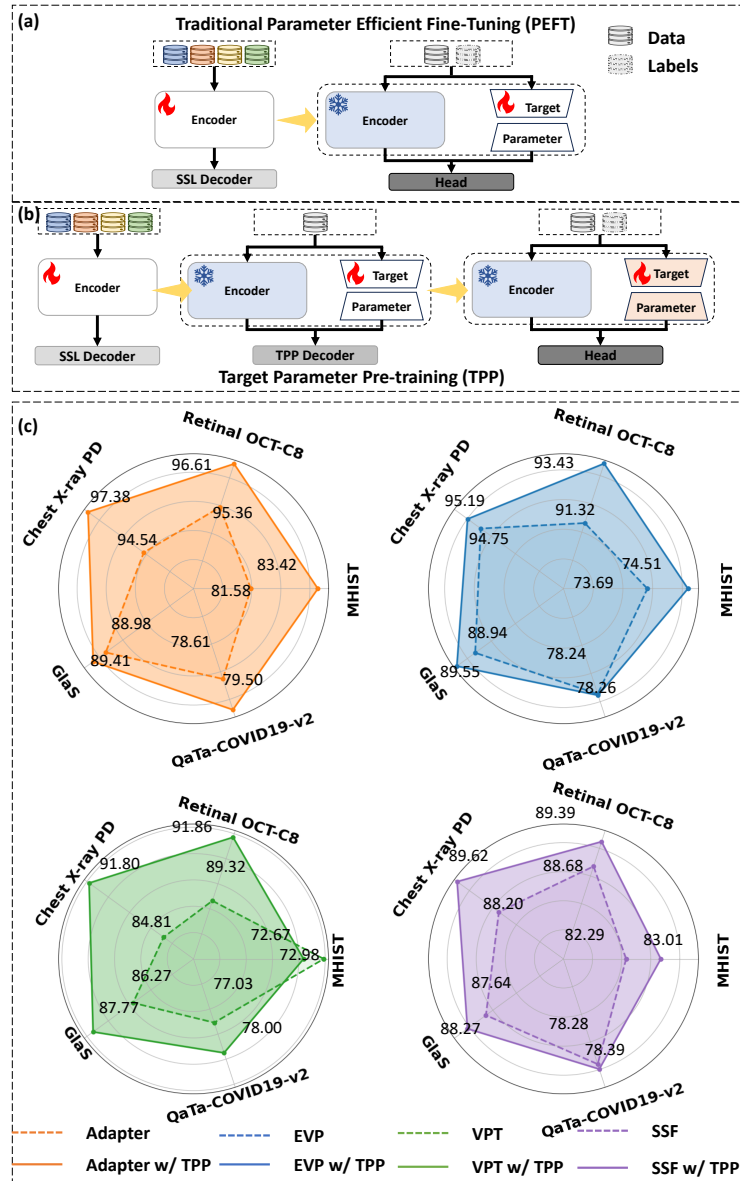


Figure 1: Comparison between (a) Traditional SSL paradigm, *i.e.*, pre-training then fine-tuning, and (b) Our TPP framework. The newly introduced stage is inserted between the pre-training stage and fine-tuning stage and is used to pre-train the target parameters. (c) Performance comparison of PEFT methods and these methods with TPP based on MAE on MedCoSS, represented by using dashed and solid lines, respectively. The different colors represent different PEFT methods.

This approach can be problematic for medical imaging tasks with limited fine-tuning data, as updating all pre-trained parameters on a small dataset can compromise model robustness and elevate the risk of overfitting Dutt et al. (2024).

To address these challenges, parameter-efficient fine-tuning (PEFT) has emerged as a promising solution Dutt et al. (2024). PEFT typically involves freezing pre-trained parameters and either updating a subset of these parameters Zaken, Goldberg and Ravfogel (2022); Touvron, Cord, El-Nouby, Verbeek and Jégou (2022) or adding a small set of new trainable parameters, known as *target parameters* Hu, Shen, Wallis, Allen-Zhu, Li, Wang, Wang, Chen et al. (2022); Houlsby, Giurgiu, Jastrzebski, Morrone, De Laroussilhe, Gesmundo, Attariyan and Gelly (2019); Chen, Ge, Tong, Wang, Song, Wang and Luo (2022); Fu, Zhu and Wu (2024); Sung, Cho and Bansal (2022); Jia, Tang, Chen,

Cardie, Belongie, Hariharan and Lim (2022); Li and Liang (2021); Wang, Cheng, Fang, Zhang, Duan and Wang (2024); He, Wu, Wang, Li and Fu (2025) (see Figure 1(a)). Methods that add target parameters have demonstrated superior performance while utilize only a small number of new parameters. However, despite leveraging the robust representations of pre-trained models, these methods do not fully exploit the benefits of pre-training. We argue that *if the backbone is pre-trained, the newly added parameters should also undergo pre-training*.

In this paper, we propose Target Parameter Pre-training (TPP), a simple yet effective fine-tuning framework. Our TPP framework focuses on pre-training the new parameters introduced by PEFT methods, excluding task-specific heads (*i.e.*, linear layers for classification or decoders for segmentation), which we refer to as target parameters. Unlike existing PEFT strategies that directly fine-tune pre-trained models with randomly initialized target parameters, our approach introduces a target parameter pre-training stage between pre-training and fine-tuning (see Figure 1(b)). This stage involves pre-training the target parameters by freezing the well-pre-trained backbone and updating the target parameters through a pretext task. Specifically, we pre-train the target parameters for each downstream dataset using its training data, enabling them to learn dataset-specific representations. Simultaneously, by integrating new knowledge into the target parameters, our approach enhances the overall representational capacity of the model. We evaluated our TPP framework on seven public datasets, comparing its performance with seven PEFT methods, full fine-tuning, and linear probe. As a plug-and-play solution, TPP can be integrated into pre-trained backbones and consistently improves existing PEFT methods (see Figure 1(c)).

The contributions of this work are three-fold.

- We propose TPP, a plug-and-play PEFT framework for medical image classification and segmentation tasks. This framework can be easily integrated into existing PEFT methods that add target parameters without requiring architectural modifications.
- We introduce the insight that if the backbone is pre-trained, the target parameters should also be pre-trained, and therefore propose a TPP stage that optimizes target parameters for specific downstream data.
- We comprehensively demonstrate that the proposed TPP framework consistently enhances PEFT baselines across seven datasets, covering two task types and four imaging modalities.

2. Related Work

2.1. PEFT Techniques

PEFT techniques aim to minimize the number of updated parameters. An initial approach involves updating specific pre-trained model parameters, such as biases Zaken et al. (2022), layer normalization Basu, Hu, Massiceti and Feizi (2024), batch normalization Frankle, Schwab and Morcos (2020), and attention mechanisms Touvron et al. (2022). However, this can disrupt the pre-trained knowledge, potentially leading to suboptimal performance.

To address this issue, recent research has focused on introducing new trainable parameters, termed target parameters. In this strategy, the parameters of the pre-trained backbone are kept fixed while the target parameters are updated using downstream datasets. This strategy can be broadly categorized into four main approaches. (1) **Adapter-based methods:** These methods Houlsby et al. (2019); Chen et al. (2022); Chen, Tao, Zhang, Wang, Li, Ye, Wang, Hu and Savvides (2024); Wang, Shen, Chen, Jiao, Liu, Zhang, Song and Li (2023) insert additional blocks in parallel or serially to learn residual features. For instance, Adapter Houlsby et al. (2019) inserts a bottleneck block with residual connections serially between the feed-forward layer of Transformer block. AdaptFormer Chen et al. (2022) employs a similar bottleneck structure without residual connections, placed in parallel within the MLP section of Transformer blocks. (2) **Low-Rank Adaptation-based (LoRA) methods:** These methods Hu et al. (2022); Zhang, Chen, Bukharin, He, Cheng, Chen and Zhao (2023); Zhong, Tang, He, Fang and Yuan (2024); Pan, Liu, Diao, Pi, Zhang, Han and Zhang (2025) introduce learnable low-rank matrices into the self-attention layers of Transformers. LoRA Hu et al. (2022) offers high parameter efficiency and integrates seamlessly with the pre-trained backbone during inference, minimizing additional computational overhead. Variants such as ConvLoRA Zhong et al. (2024) and AdaLoRA Zhang et al. (2023) enhance LoRA by incorporating lightweight convolutional parameters or adaptively allocating parameter budgets based on importance scores. (3) **Prompting-based methods:** These methods Jia et al. (2022); He et al. (2025); Yoo, Kim, Jung, Lee and Yoon (2023); Wang et al. (2024) modify the input to Transformer layers by adding learnable tokens. For example, VPT Jia et al. (2022) and its variants He et al. (2025); Yoo et al. (2023) introduce learnable tokens to the inputs of Transformer layers for visual tasks. Although parameter-efficient, these methods can be sensitive to prompt

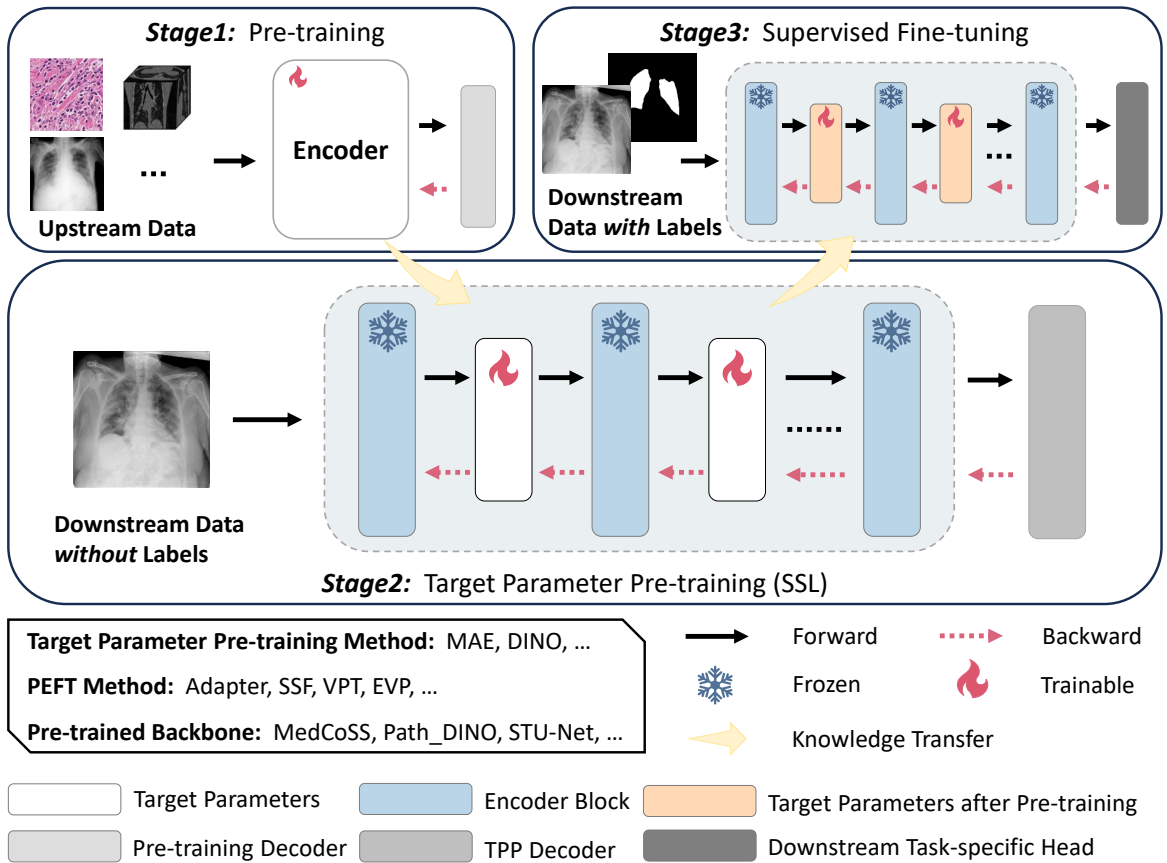


Figure 2: Overview of the proposed TPP framework. It introduces a pre-training stage for target parameters between the traditional pre-training and the subsequent supervised fine-tuning stages.

token lengths and may exhibit suboptimal performance when applied to self-supervised pre-trained backbones. (4) **Side-tuning-based methods:** These methods Huang, Cheng, Tam and Tang (2024); Fu et al. (2024); Yin, Han, Li, Feng and Bai (2024); Tang, Fu, Zhu and Wu (2024) utilize a separate side model that operates independently of the frozen backbone, avoiding gradient backpropagation through the backbone. For instance, DTL Fu et al. (2024) uses a lightweight Compact Side Network (CSN) with low-rank linear mappings to capture task-specific features, which are then integrated into the backbone.

Despite the progress in PEFT, many existing methods initialize target parameters randomly (*e.g.*, using zero, uniform distributions, or normal distributions) Houlsby et al. (2019); Hu et al. (2022); Lian, Zhou, Feng and Wang (2022); Jia et al. (2022). For instance, LoRA typically initializes its two low-rank matrices with zero and random values, respectively. These methods aim to ensure that target parameters do not alter the input to the original layer initially Liao, Tan and Monz (2024). However, this approach overlooks the potential benefits of pre-training for these new parameters. Given the established advantages of pre-training for backbone parameters, it is reasonable to expect similar benefits for target parameters.

Recent efforts have explored improving target parameter initialization. Self-Prompt Tuning Wang et al. (2024) initializes prompts using token prototypes derived from target data, specifically for prompting-based methods. PVP Song, Yang, Guan, Zhu, Qiao and Hu (2023) pre-trains target parameters on a large-scale dataset, and Su *et al.* Su, Wang, Qin, Chan, Lin, Wang, Wen, Liu, Li, Li et al. (2022) initializes target parameters with soft prompts pre-trained on related tasks. However, these methods do not fully address the challenge of selecting appropriate datasets for pre-training target parameters. We argue that pre-training directly on the target dataset offers a more practical and effective

solution. Therefore, our proposed TPP framework pre-trains target parameters using the current target training data to enhance subsequent fine-tuning performance.

Cekmeceli *et al.* Cekmeceli, Himmetoglu, Tombak, Susmelj, Erdil and Konukoglu (2024) investigated the domain generalization performance of foundation models fine-tuned with various PEFT methods, emphasizing the importance of selecting appropriate techniques to ensure that target parameters trained on source domain data can be directly applied to target domain data. In contrast, our work focuses on the broad impact of target parameter initialization on performance in target tasks.

2.2. SSL Methods

SSL is a powerful technique for representation learning Chen et al. (2020); He, Fan, Wu, Xie and Girshick (2020); Caron, Touvron, Misra, Jégou, Mairal, Bojanowski and Joulin (2021); Michelucci (2022); Vincent, Larochelle, Bengio and Manzagol (2008); He, Chen, Xie, Li, Dollár and Girshick (2022). SSL typically consists of two stages: unsupervised pre-training on a large scale unlabeled data with a pretext task and supervised fine-tuning on target data.

Various pretext tasks have been explored, including contrastive learning Chen et al. (2020); He et al. (2020); Caron et al. (2021) and generative learning Michelucci (2022); Vincent et al. (2008); He et al. (2022), as well as combinations thereof Goodfellow, Pouget-Abadie, Mirza, Xu, Warde-Farley, Ozair, Courville and Bengio (2020). For instance, Masked Autoencoders (MAE) He et al. (2022) employs masked image modeling, where an image is divided into patches, most of which are randomly masked. The model learns to predict these masked patches from the remaining visible ones. DINO Caron et al. (2021) combines multi-crop learning Caron, Misra, Mairal, Goyal, Bojanowski and Joulin (2020) with self-distillation for contrastive learning, utilizing centering and sharpening operations to prevent collapse in the momentum teacher model's output vectors. SSL pre-training enables models to learn high-quality representations, reducing the reliance on large annotated datasets and accelerating convergence. This is particularly valuable for various medical image analysis tasks, including classification Zhou, Lu, Yang, Han and Yu (2021); Ye et al. (2024), localization Yang, Wu, Zhou and Lin (2021); Siméoni, Puy, Vo, Roburin, Gidaris, Bursuc, Pérez, Marlet and Ponce (2021), and segmentation Zhou et al. (2021); Ye et al. (2024); Ye, Zhang, Chen and Xia (2022).

Despite the benefits of SSL for pre-training backbones, PEFT methods often initialize new parameters randomly, potentially undermining these benefits. To address this, our study introduces an additional pre-training stage for these new parameters before fine-tuning, aiming to fully leverage the potential of SSL.

3. Method

3.1. Preliminaries

Paradigm of SSL. SSL typically involves two stages: pre-training and fine-tuning. Let D_{un} denote a large-scale unlabeled dataset, and θ represent the parameters of the backbone network. In the pre-training stage, θ is trained on D_{un} by completing a pretext task that does not require human-labeled data for supervision. The parameters obtained after pre-training, denoted as θ^p , exhibit strong transferability to various downstream tasks. In the fine-tuning stage, a labeled dataset D_l is used to adapt the pre-trained backbone to the target task. This is achieved by adding a new task-specific head, represented by θ_{head} , and updating all parameters. The process of a single feed-forward operation is described as:

$$P = f(I, \langle \theta^p, \theta_{head} \rangle), I \in D_l, \quad (1)$$

where I is the input image, $\langle \cdot \rangle$ denotes the set of parameters involved in the feed-forward process $f(\cdot)$, and P is the output.

Pre-trained Backbone. We primarily employ MedCoSS Ye et al. (2024) as the pre-trained backbone, due to its large-scale multi-modal pre-training and robust generalization ability across downstream tasks with various modalities. MedCoSS is based on ViT/B Dosovitskiy, Beyer, Kolesnikov, Weissenborn, Zhai, Unterthiner, Dehghani, Minderer, Heigold, Gelly et al. (2020) and pre-trained using the pretext task of masked modeling Devlin, Chang, Lee and Toutanova (2019); He et al. (2022). To demonstrate the general applicability of TPP, we also experimented with two additional backbones: Path_DINO Kang et al. (2023), which is pre-trained on pathological images using DINO Caron et al. (2021), and STU-Net Huang, Wang, Deng, Ye, Su, Sun, He, Gu, Gu, Zhang et al. (2023), a CNN-based medical foundation model pre-trained on the TotalSegmentator dataset Wasserthal, Breit, Meyer, Pradella, Hinck, Sauter, Heye, Boll, Cyriac, Yang et al. (2023) in a supervised learning manner.

Table 1

Overview of the datasets used in this study.

Dataset	Modality	Task	Train	Val	Test
MHIST	Path.	Cls	1740	435	977
Retinal OCT-C8	OCT	Cls	18400	2800	2800
Chest X-ray PA	X-ray	Cls	3201	459	915
GlaS	Path.	Seg	67	18	80
QaTa	X-ray	Seg	5716	1429	2113

Table 2

Implementation details of five downstream tasks. CE: cross-entropy loss function.

Dataset	Loss Function	Patch Size	Learning Rate	Batch Size	Iterations
MHIST	CE	224 × 224	Grid Search	32	2,700
Retinal OCT-C8	CE	224 × 224	0.0001	32	57,500
Chest X-ray PA	CE	224 × 224	0.0001	32	1,980
GlaS	Dice+CE	512 × 512	0.0001	4	25,000
QaTa	Dice+CE	224 × 224	0.0001	16	25,000

PEFT based on Adding New Parameters. Leveraging the representation capabilities of pre-trained models, effective PEFT can be achieved by freezing the pre-trained model parameters and introducing new trainable parameters, termed target parameters θ_{tp} . The feed-forward process can then be described as:

$$P = f(I, \langle |\theta^p|, \theta_{tp}, \theta_{head} \rangle), I \in D_I, \quad (2)$$

where $|\cdot|$ indicates the frozen parameters.

3.2. Target Parameter Pre-training

To address the limitations of randomly initialized target parameters, which may not fully exploit the benefits of pre-training, we introduce a TPP stage between the self-supervised pre-training and fully-supervised fine-tuning, as depicted in Figure 2. During TPP, we freeze the pre-trained backbone parameters θ^p , while keeping the target parameters θ_{tp} trainable. Given a target dataset D_I , we pre-train θ_{tp} by performing a defined pretext task. We explored two popular pretext tasks, MAE He et al. (2022) and DINO Caron et al. (2021), to validate the effectiveness of TPP. Empirically, TPP based on MAE generally outperforms TPP based on DINO across most PEFT methods. We now delve in the details.

TPP based on MAE. MAE is a generative SSL pretext task that divides an image into multiple non-overlapping patches, randomly masks a significant portion (typically 75%), and uses the visible patches to predict the masked ones. A mean squared error (MSE) loss function is used to minimize prediction errors. This task exploits the redundancy in images, forcing the model to learn rich contextual representations that capture both local and global features.

TPP based on DINO. DINO is a contrastive SSL pretext task. For an image, strong data augmentations are used to generate two distinct views, which are processed by both the student and teacher models. The student model is a pre-training backbone followed by multi-layer perceptrons (MLPs), while the teacher model is a momentum-updated version of the student model. The student model is trained to maximize the similarity of the output vectors to those of the teacher model using a cross-entropy loss function.

Using both SSL pretext tasks, we obtain the pre-trained target parameters θ_{tp}^p . These parameters, along with θ^p , are then transferred to the target dataset D_I . Following PEFT methods, we freeze θ^p and keep θ_{tp}^p and θ_{head} trainable. The feed-forward process is defined as:

$$P = f(I, \langle |\theta^p|, \theta_{tp}^p, \theta_{head} \rangle), I \in D_I. \quad (3)$$

Our TPP framework is designed to be a plug-and-play solution, seamlessly integrating with any PEFT method that utilizes target parameters without requiring architectural modifications.

Table 3

Results of Adapter with TPP, full fine-tuning, linear probe, and seven PEFT methods on three classification downstream tasks. The best result on each column is highlighted in **bold**. Ratio denotes the ratio of trainable parameters to total parameters.

Method	MHIST				Retinal OCT-C8				Chest X-ray PA			
	ACC	AUC	F1	Ratio	ACC	AUC	F1	Ratio	ACC	AUC	F1	Ratio
full fine-tuning	83.11	89.78	81.60	100.0	94.54	99.64	94.53	100.0	93.33	98.97	93.34	100.0
linear probe	68.99	77.08	66.46	0.003	59.96	92.64	59.42	0.008	74.97	97.45	70.03	0.004
EVP	73.69	81.34	71.82	0.961	91.32	99.34	91.31	0.966	94.75	99.21	94.72	0.962
VPT	72.98	79.84	71.35	0.103	89.32	99.04	89.25	0.108	84.81	95.33	84.58	0.103
SSF	82.29	89.29	80.85	0.172	88.68	98.93	88.66	0.177	88.20	97.78	87.81	0.173
BitFit	82.40	89.60	80.86	0.115	87.18	98.81	87.13	0.120	87.65	98.19	87.18	0.116
Adapter	81.58	89.09	80.16	3.045	95.36	99.74	95.36	3.050	94.54	99.50	94.48	3.046
AdaptFormer	66.02	74.30	65.07	3.831	82.32	98.11	82.37	3.836	79.23	92.77	78.95	3.832
DTL	77.48	84.85	75.09	0.051	89.79	99.13	89.81	0.055	90.71	98.40	90.51	0.051
Adapter w/ TPP	83.42	91.38	82.21	3.045	96.61	99.77	96.61	3.050	97.38	99.63	97.37	3.046

Table 4

Results of Adapter with TPP, full fine-tuning, linear probe, and seven PEFT methods on two segmentation downstream tasks. The best result on each column is highlighted in **bold**. Ratio denotes the ratio of trainable parameters to total parameters.

Method	GlaS			QaTa		
	Dice	HD	Ratio	Dice	HD	Ratio
full fine-tuning	88.84	47.41	100.0	78.63	29.54	100.0
linear probe	86.56	61.85	2.000	73.62	39.46	2.000
EVP	88.94	49.10	2.940	78.24	31.67	2.940
VPT	86.27	52.23	2.100	77.03	33.43	2.100
SSF	87.64	54.49	2.170	78.28	30.53	2.170
BitFit	87.56	58.58	2.110	77.99	32.30	2.110
Adapter	88.98	49.06	4.980	78.61	29.91	4.980
AdaptFormer	86.62	61.43	5.750	74.97	36.23	5.750
DTL	87.52	55.11	2.047	73.99	38.29	2.047
Adapter w/ TPP	89.41	44.25	4.980	79.50	29.28	4.980

Table 5

Results on four PEFT Methods based on TPP. For TPP, we used MAE as the pretext task. We highlight in **bold** the better results comparing each PEFT method with and without TPP.

Method	MHIST			Retinal OCT-C8			Chest X-ray PA			GlaS		QaTa	
	ACC	AUC	F1	ACC	AUC	F1	ACC	AUC	F1	Dice	HD	Dice	HD
Adapter	81.58	89.09	80.16	95.36	99.74	95.36	94.54	99.50	94.48	88.98	49.06	78.61	29.91
Adapter w/ TPP	83.42	91.38	82.21	96.61	99.77	96.61	97.38	99.63	97.37	89.41	44.25	79.50	29.28
EVP	73.69	81.34	71.82	91.32	99.34	91.31	94.75	99.21	94.72	88.94	49.10	78.24	31.67
EVP w/ TPP	74.51	82.17	72.13	93.43	99.47	93.43	95.19	99.36	95.18	89.55	48.06	78.26	31.23
VPT	72.98	79.84	71.35	89.32	99.04	89.25	84.81	95.33	84.58	86.27	52.23	77.03	33.43
VPT w/ TPP	72.67	80.19	71.55	91.86	99.28	91.85	91.80	98.71	91.66	87.77	57.06	78.00	31.98
SSF	82.29	89.29	80.85	88.68	98.93	88.66	88.20	97.78	87.81	87.64	54.49	78.28	30.53
SSF w/ TPP	83.01	90.50	81.72	89.39	99.05	89.35	89.62	98.44	89.26	88.27	57.36	78.39	31.09

4. Experiments

4.1. Datasets

The TPP framework was evaluated on five downstream datasets: MHIST Wei, Suriawinata, Ren, Liu, Lisovsky, Vaickus, Brown, Baker, Tomita, Torresani et al. (2021), Retinal OCT-C8 Subramanian, Shanmugavadivel, Naren, Premkumar and Rankish (2022), Chest X-ray PA Asraf and Islam (2021), GlaS Sirinukunwattana, Pluim, Chen, Qi,

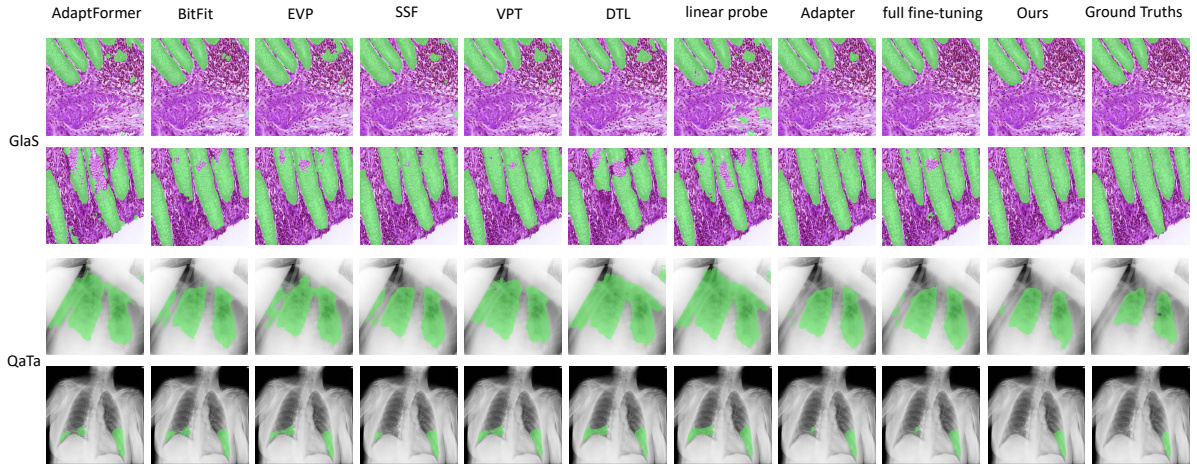


Figure 3: Visualization of segmentation results obtained by AdaptFormer, BitFit, EVP, SSF, VPT, DTL, linear probe, Adapter, full fine-tuning, Ours, and Ground Truths. The pneumonia and malignant regions are colored green.

Table 6

Results on three PEFT methods based on TPP. For TPP, we used DINO as the pretext task. We highlight in **bold** the better results comparing each PEFT method with and without TPP.

	MHIST			Retinal OCT-C8			GlaS		QaTa	
	ACC	AUC	F1	ACC	AUC	F1	Dice	HD	Dice	HD
Adapter	81.58	89.09	80.16	95.36	99.74	95.36	88.98	49.06	78.64	30.54
Adapter w/ TPP	82.29	88.59	81.29	96.25	99.75	96.24	88.60	46.98	79.11	29.27
VPT	72.98	79.84	71.35	89.32	99.04	89.25	86.27	52.23	77.03	33.43
VPT w/ TPP	74.31	81.21	71.97	91.14	99.24	91.13	87.06	58.63	77.06	32.81
SSF	82.29	89.29	80.85	88.68	98.93	88.66	87.64	54.49	78.28	30.53
SSF w/ TPP	83.32	90.69	82.04	89.82	99.12	89.81	88.07	56.43	78.61	30.97

Table 7

Results of Adapter and different TPP variants with pre-training on one dataset and fine-tuning on another dataset. The pretext task is MAE and the fine-tuning framework is Adapter. The best result on each column is highlighted in **bold**.

	Modality	MHIST			GlaS		Chest X-ray PA			QaTa		Retinal OCT-C8		
		ACC	AUC	F1	Dice	HD	ACC	AUC	F1	Dice	HD	ACC	AUC	F1
MHIST	Path.	83.42	91.38	82.21	89.65	45.54	95.74	99.62	95.71	78.84	29.69	96.00	99.74	95.99
GlaS		82.40	89.56	81.25	89.41	44.25	95.08	99.55	95.07	78.99	29.72	96.07	99.74	96.07
Chest X-ray PA	X-ray	79.12	88.16	78.04	88.51	50.36	97.38	99.63	97.37	78.76	30.13	95.71	99.78	95.72
QaTa		79.63	87.96	78.30	89.20	44.27	94.97	99.24	94.95	79.50	29.28	95.89	99.74	95.88
Retinal OCT-C8	OCT	81.78	89.32	80.06	88.32	47.75	95.19	99.56	95.15	78.68	30.23	96.61	99.77	96.61
Adapter	-	81.58	89.09	80.16	88.98	49.06	94.54	99.50	94.48	78.61	29.91	95.36	99.74	95.36

Heng, Guo, Wang, Matuszewski, Bruni, Sanchez et al. (2017), and QaTa-COVID19-v2 (QaTa) Degerli, Kiranyaz, Chowdhury and Gabbouj (2022). Detailed information for these datasets is available in Table 1. **MHIST Dataset Wei et al. (2021):** For the classification task, this dataset includes 3,152 colorectal polyp images, categorized into hyperplastic polyps (HP) and sessile serrated adenomas (SSA), with 2,175 training and 977 test images. Following the official data splits, 20% of the training data from each category was randomly selected for validation. **Retinal OCT-C8 Dataset Subramanian et al. (2022):** For the classification task, this dataset contains 24,000 optical coherence tomography (OCT) 2D images in eight categories: age-related macular degeneration (AMD), choroidal neovascularization (CNV), central serous retinopathy (CSR), diabetic macular edema (DME), macular hole (MH), choroidal drusen (DRUSEN), diabetic retinopathy (DR), and normal retina (NORMAL). The official data split was

Table 8

Results on different initialization strategies. We used Adapter as the baseline. Transfer means initializing target parameters by pre-training on a larger, similar dataset. Upstream means initializing target parameters by pre-training on upstream data. The best result on each column is highlighted in **bold**.

	MHIST			Retinal OCT-C8			GlaS		QaTa	
	ACC	AUC	F1	ACC	AUC	F1	Dice	HD	Dice	HD
Random	81.58	89.09	80.16	95.36	99.74	95.36	88.98	49.06	78.61	29.91
Transfer	82.91	89.51	81.38	94.61	99.66	94.62	89.46	42.85	79.13	29.93
TPP w/ DINO	82.29	88.59	81.29	96.25	99.75	96.24	88.60	46.98	79.11	29.27
TPP w/ MAE	83.42	91.38	82.21	96.61	99.77	96.61	89.41	44.25	79.50	29.28
Upstream	82.09	89.59	79.97	-	-	-	89.28	44.66	79.34	29.28

used for training, validation, and test sets. **Chest X-ray PA Dataset Asraf and Islam (2021)**: For the classification task, this dataset comprises 4,575 2D chest X-ray images categorized into COVID-19 infections, other pneumonia infections, and healthy controls. Due to the absence of official splits, the data was randomly divided into 70% for training, 10% for validation, and 20% for testing from each category. **GlaS Dataset Sirinukunwattana et al. (2017)**: For the segmentation task, this dataset contains 165 pathological images of H&E-stained colon tissue sections, labeled as malignant or benign. The official data splits were followed, and 20% of the training data from each category was randomly selected for validation. **QaTa-COV19v2(QaTa) Dataset Degerli et al. (2022)**: For the segmentation task, this dataset is used for segmenting COVID-19 infected regions. It consists of 7,145 training images and 2,113 test images. The official data splits were used, and 20% of the training samples were allocated to form the validation set.

4.2. Implementation Details

TPP based on MAE. For target parameter pre-training with MAE, we adopted the methodology detailed in Ye et al. (2024); He et al. (2022). The AdamW optimizer was employed with a learning rate of $1.5e-3$, a weight decay of $1.5e-2$, and a batch size of 64. Pre-training was conducted for a maximum of 500 epochs for classification tasks and 1000 epochs for segmentation tasks, with the latter requiring more epochs due to smaller dataset sizes. A warm-up strategy over the initial 40 epochs linearly increased the learning rate to $1.5e-3$, followed by a cosine decay to zero.

TPP based on DINO. For target parameter pre-training with DINO, we followed the configuration in Caron et al. (2021). The AdamW optimizer was used with a batch size of 64. The learning rate underwent a linear warm-up over the first 10 epochs, increasing to a base value determined by the linear scaling rule: $lr=0.0001 \times \text{batch size}/256$, followed by a cosine decay. Similarly, weight decay followed a cosine schedule from 0.04 to 0.4. Data augmentations consistent with DINO, including color jittering, Gaussian blur, and solarization, were applied.

Downstream Fine-tuning Stage. During fine-tuning, we followed the framework by MedCoSS Ye et al. (2024), using TPP based on MAE as the default configuration. Experiments were also conducted with TPP based on DINO. The AdamW optimizer was utilized with hyperparameters specific to each downstream task. Table 2 presents the implementation details for the five downstream datasets, including loss functions, patch sizes, learning rates, batch sizes, and maximum iterations. For MHIST, a grid search for the learning rate between 0.000005 and 0.05 was performed due to the sensitivity of PEFT methods. The learning rates for full fine-tuning, linear probe, EVP, VPT, SSF, BitFit, Adapter, AdaptFormer, and DTL were set to 0.00001, 0.01, 0.00005, 0.0001, 0.001, 0.001, 0.0001, 0.001, and 0.005, respectively.

Image Sizes of the Datasets. Images in MHIST and QaTa are originally 224×224 pixels. For Retinal OCT-C8, image sizes range from 384×496 to 1536×496 pixels. All images were resized to 224×224 pixels for uniformity. Similarly, Chest X-ray PA images, with original sizes from 224×224 to 5623×4757 pixels, were uniformly resized to 224×224 pixels. The GlaS dataset, initially 522×775 pixels, was resized to 512×512 pixels.

4.3. Evaluation Metrics

For classification tasks, we used the area under the receiver operator curve (AUC, %), accuracy (ACC, %), and F1 score (F1, %) as evaluation metrics. For segmentation tasks, performance was evaluated using the Dice similarity coefficient (Dice, %) and the 95% Hausdorff distance (HD).

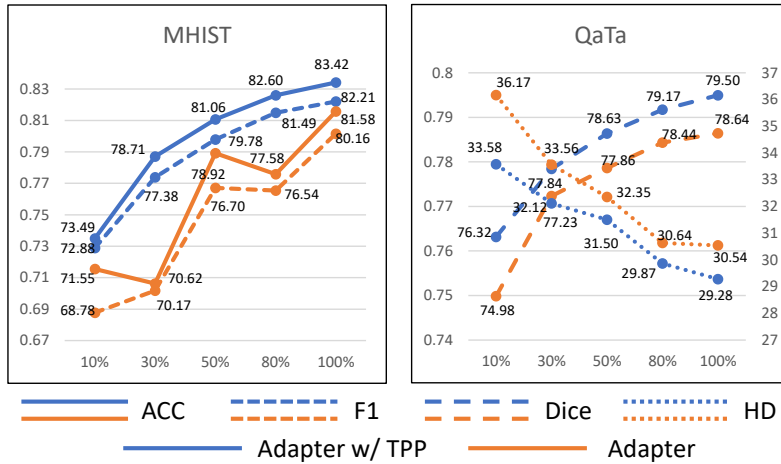


Figure 4: Results of Adapter with and without TPP on the MHIST and QaTa with 10%, 30%, 50%, 80%, and 100% training data.

4.4. Comparisons with State-of-the-art Methods

We compared Adapter with TPP against nine methods, including full fine-tuning, linear probe, EVP Liu, Shen, Pun and Cun (2023), VPT Jia et al. (2022), SSF Lian et al. (2022), BitFit Zaken et al. (2022), Adapter Housley et al. (2019), AdaptFormer Chen et al. (2022), and DTL Fu et al. (2024), on the MHIST, Retinal OCT-C8, Chest X-ray PA, GlaS, and QaTa datasets. MedCoSS served as the pre-trained backbone. Full fine-tuning updates all model parameters, while linear probe only updates the task-specific head. The results in Tables 3 and Table 4 indicate the following: (1) Among the PEFT methods, Adapter achieves the best generalization performance across all datasets. (2) Applying the proposed TPP to Adapter leads to significant performance improvements on all datasets. For instance, TPP enhances Adapter’s performance on MHIST by 1.84% (ACC), 2.29% (AUC), and 2.05% (F1). On GlaS, TPP improves Dice by 0.43% and HD by 4.81 pixels. (3) Adapter with TPP outperforms full fine-tuning on MHIST, Retinal OCT-C8, Chest X-ray PA, GlaS, and QaTa, while updating approximately 3%, 3%, 3%, 5%, and 5% of the parameters, respectively.

For qualitative comparison, Figure. 3 visualizes the segmentation results of AdaptFormer, BitFit, EVP, SSF, VPT, DTL, linear probe, Adapter, full fine-tuning, and our proposed method (Adapter with TPP) on the GlaS and QaTa datasets. These visualizations demonstrate that the segmentation results of our approach more closely match the ground truth, effectively mitigating both over- and under-segmentation. For instance, in the second row, all competing methods exhibit under-segmentation of glandular tissue, whereas our TPP method achieves more accurate segmentation. Notably, compared to full fine-tuning, our method achieves comparable results in the first row and more accurate results in the subsequent rows.

4.5. Other PEFT Methods with TPP

To further validate the effectiveness of TPP, we extended its application to three additional PEFT methods: EVP, VPT, and SSF, and reported their performance with and without TPP. MedCoSS was used as the pre-trained backbone. The results in Table 5 confirm the robustness of our TPP approach, showing consistent positive effects across most metrics and datasets. For instance, the combination of EVP with TPP surpasses the performance of EVP alone across all datasets, including both classification and segmentation tasks. Specifically, on MHIST, EVP combined with TPP yields performance improvements of 0.82% (ACC), 0.83% (AUC), and 0.31% (F1) compared to EVP alone. Similarly, on GlaS, adding TPP to EVP results in gains of 0.61% in Dice and 1.04 pixels in HD over EVP.

4.6. TPP based on DINO

While the default pre-training pretext task for TPP is MAE, we also employed DINO Caron et al. (2021) as the pretext task and evaluated three PEFT methods: Adapter, VPT, and SSF, as summarized in Table 6. MedCoSS served as the pre-trained backbone. The results demonstrate that TPP, when using DINO, also enhanced fine-tuning performance, achieving superior results across nearly all metrics. For instance, Adapter with TPP achieves improvements of 0.89% (Retinal OCT-C8 ACC), 0.88% (Retinal OCT-C8 F1), 0.47% (QaTa Dice), and 1.27 pixels (QaTa HD).

Table 9

Results for TPP based on MAE on MHIST and QaTa with the Path_DINO backbone. The best result on each task is highlighted in **bold**.

	MHIST			QaTa	
	ACC	AUC	F1	Dice	HD
Adapter	82.91	90.79	80.99	80.20	26.92
Adapter w/ TPP	85.67	92.84	83.94	80.37	26.54
VPT	81.99	88.39	80.39	79.62	29.38
VPT w/ TPP	82.40	90.02	80.20	79.80	28.82

5. Discussion

5.1. Fine-tuning with Fewer Annotations

We evaluated the performance of Adapter, with and without TPP, on the MHIST and QaTa datasets by progressively increasing the ratios of training annotations from 10% to 100%, as depicted in Figure 4. MedCoSS was the pre-trained backbone. As the amount of training data increased, the model’s performance generally improves. Throughout this process, Adapter with TPP consistently outperforms Adapter on both the classification dataset MHIST and the segmentation dataset QaTa, demonstrating the effectiveness of TPP across varying amounts of training annotations.

5.2. Target Parameter Pre-training on Other Data

TPP directly utilizes the target training data for pre-training. In this section, we further investigated the performance impact of using other datasets for pre-training in a cross-validation setting. TPP with MAE was the pre-training strategy, and MedCoSS was the pre-trained backbone. Specifically, we selected five datasets spanning three modalities for evaluation and pre-trained TPP on one dataset before fine-tuning the pre-trained model on all datasets. The baseline performance of Adapter was also recorded. The results are shown in Table 7. We observed that TPP achieved superior performance when the pre-training and fine-tuning data shared identical modalities, with the best performance typically obtained when using the same dataset. Moreover, using data from a different modality for pre-training often resulted in negative effects, leading to worse performance than Adapter without TPP. For example, after pre-training adapters on the Retinal OCT-C8 dataset and fine-tuning on the GlaS dataset, we observed a 0.66% decrease in Dice performance compared to Adapter without TPP. In summary, TPP can effectively realize its potential when pre-trained on data that is either the same as or within the same modalities as the target data.

5.3. Initialization of Target Parameters

We explored various initialization strategies for target parameters, using MedCoSS as the pre-trained backbone and Adapter as the PEFT strategy. These strategies include random, transfer, TPP with DINO, TPP with MAE, and upstream. Random initialization involves initializing the target parameters with random values. Transfer learning involves initializing the target parameters by using target parameters pre-trained on a larger dataset with similar characteristics, as described in Su et al. (2022); Song et al. (2023). Specifically, we used the CRAG Awan, Sirinukunwattana, Epstein, Jefferyes, Qidwai, Aftab, Mujeeb, Snead and Rajpoot (2017), OCT2017 Kermany, Zhang, Goldbaum et al. (2018), MHIST Wei et al. (2021), and ChestXR Akhloufi and Chetoui (2021) datasets for transfer learning for the MHIST, Retinal OCT-C8, GlaS, and QaTa datasets, respectively. Upstream pre-training involves pre-training the target parameters on upstream data. For this, we utilized MedCoSS’s upstream training data, which shares the same modality as the current task. Consequently, the TCGA¹ dataset was employed as upstream data for MHIST and GlaS, while the MIMIC-CXR dataset was employed as upstream data for QaTa. This experiment was not conducted for Retinal OCT-C8 due to the absence of corresponding modality data for upstream pre-training. The results, presented in Table 8, demonstrate that pre-training-based strategies consistently outperformed random initialization, emphasizing the benefits of improved target parameter initialization. Notably, TPP with MAE achieved the best generalization performance across all datasets, highlighting its superiority.

5.4. New Backbones

To evaluate the generalization capability of our TPP, we incorporated two new pre-trained backbones: Path_DINO Kang et al. (2023) and STU-Net Huang et al. (2023). Path_DINO is a ViT-based model pre-trained on pathological

¹<https://portal.gdc.cancer.gov/>

Table 10

Results for TPP based on DINO on two 3D segmentation tasks with the STU-Net backbone. The best result on each task is highlighted in **bold**.

	LiTS			KiTS		
	Mean	Organ	Tumor	Mean	Organ	Tumor
Conv-Adapter	77.05	95.27	58.83	81.24	95.99	66.48
Conv-Adapter w/ TPP	77.95	95.25	60.64	82.73	95.81	69.66

Table 11

Comparison of Decoder Parameter Handling Strategies in TPP Based on MAE: Freezing, Updating, and Non-Inheritance on Chest X-ray PA and QaTa Datasets. The best result on each column is highlighted in **bold**.

	Chest X-ray PA			QaTa	
	ACC	AUC	F1	Dice	HD
Random	96.17	99.35	96.17	79.43	29.29
Freeze	97.38	99.63	97.37	79.01	29.45
Update	95.63	99.59	95.60	79.50	29.28

images using DINO Caron et al. (2021). We evaluated its performance with two PEFT methods: Adapter and VPT. We employed MAE as the pretext task. As shown in Table 9, the results consistently demonstrate performance improvements across various datasets and metrics. Specifically, with Adapter, TPP based on MAE achieves improvements of 2.76% (MHIST ACC), 2.05% (MHIST AUC), 2.95% (MHIST F1), 0.17% (QaTa Dice), and 0.38 pixels (QaTa HD).

STU-Net is a 3D CNN-based pre-trained model trained on the TotalSegmentator dataset Wasserthal et al. (2023) in a supervised manner. To accommodate CNN-based architectures, we employed Conv-Adapter Chen et al. (2024) as the PEFT method and DINO as the pretext task. Additionally, we introduced two 3D medical segmentation datasets, LiTS Bilic, Christ, Li, Vorontsov, Ben-Cohen, Kaissis, Szeskin, Jacobs, Mamani, Chartrand et al. (2023) and KiTS Heller, Sathianathen, Kalapara, Walczak, Moore, Kaluzniak, Rosenberg, Blake, Rengel, Oestreich et al. (2019), to evaluate the effectiveness of our TPP on CNN-based models and 3D data. As shown in Table 10, Conv-Adapter with TPP achieves superior performance in tumor segmentation, while exhibiting a slight decline in organ segmentation performance compared to its counterpart without TPP. These results highlight the effectiveness and generalizability of our proposed approach.

5.5. Decoder update strategy for TPP based on MAE

When using an MAE-based pre-trained model, its pre-trained decoder can be directly inherited. In this section, we investigated the impact of inheriting and freezing the pre-trained decoder during TPP. To this end, we conducted experiments on the Chest X-ray PA and QaTa datasets, with the results summarized in Table 11. Our findings indicate that: (1) inheriting the pre-trained decoder enhances classification performance but provides only a marginal improvement for segmentation tasks; (2) after adopting the pre-trained decoder, freezing it benefits classification tasks but negatively affects segmentation performance. Based on these observations, we chose to freeze the pre-trained decoder for classification tasks while allowing updates for segmentation tasks.

6. Conclusions

This paper introduces a novel perspective to enhance the performance of PEFT methods. Driven by the principle that *if the backbone is pre-trained, the newly introduced parameters should also be pre-trained*, we propose TPP, a plug-and-play fine-tuning framework for medical image analysis. TPP incorporates an additional pre-training stage before fine-tuning, specifically designed to pre-train the new parameters introduced by PEFT methods. The proposed framework exhibits high flexibility, supporting various pre-trained backbones, diverse pretext tasks for target parameter pre-training, and various PEFT techniques. Extensive experiments across seven datasets, covering both classification and segmentation tasks, demonstrate the consistent effectiveness of TPP. Future work will focus on designing targeted pretext strategies for target parameter pre-training, aiming to establish a unified and effective approach to fully leverage pre-training benefits for newly introduced parameters.

References

- Akhlooui, M.A., Chetoui, M., 2021. Chest XR COVID-19 detection. <https://cxr-covid19.grand-challenge.org/>. Online; accessed September 2021.
- Asraf, A., Islam, Z., 2021. Covid19, pneumonia and normal chest x-ray pa dataset. mendeley data v1 (2021).
- Awan, R., Sirinukunwattana, K., Epstein, D., Jefferys, S., Qidwai, U., Aftab, Z., Mujeeb, I., Snead, D., Rajpoot, N., 2017. Glandular morphometrics for objective grading of colorectal adenocarcinoma histology images. *Scientific reports* 7, 16852.
- Azizi, S., Mustafa, B., Ryan, F., Beaver, Z., Freyberg, J., Deaton, J., Loh, A., Karthikesalingam, A., Kornblith, S., Chen, T., et al., 2021. Big self-supervised models advance medical image classification, in: *Proceedings of the IEEE/CVF international conference on computer vision*, pp. 3478–3488.
- Basu, S., Hu, S., Massiceti, D., Feizi, S., 2024. Strong baselines for parameter-efficient few-shot fine-tuning, in: *Proceedings of the AAAI Conference on Artificial Intelligence*, pp. 11024–11031.
- Bilic, P., Christ, P., Li, H.B., Vorontsov, E., Ben-Cohen, A., Kaissis, G., Szeskin, A., Jacobs, C., Mamani, G.E.H., Chartrand, G., et al., 2023. The liver tumor segmentation benchmark (lits). *Medical image analysis* 84, 102680.
- Caron, M., Misra, I., Mairal, J., Goyal, P., Bojanowski, P., Joulin, A., 2020. Unsupervised learning of visual features by contrasting cluster assignments. *Advances in neural information processing systems* 33, 9912–9924.
- Caron, M., Touvron, H., Misra, I., Jégou, H., Mairal, J., Bojanowski, P., Joulin, A., 2021. Emerging properties in self-supervised vision transformers, in: *Proceedings of the IEEE/CVF international conference on computer vision*, pp. 9650–9660.
- Cekmeceli, K., Himmetoglu, M., Tombak, G.I., Susmelj, A., Erdil, E., Konukoglu, E., 2024. Do vision foundation models enhance domain generalization in medical image segmentation? *arXiv preprint arXiv:2409.07960*.
- Chen, H., Tao, R., Zhang, H., Wang, Y., Li, X., Ye, W., Wang, J., Hu, G., Savvides, M., 2024. Conv-adapter: Exploring parameter efficient transfer learning for convnets, in: *Proceedings of the IEEE/CVF Conference on Computer Vision and Pattern Recognition*, pp. 1551–1561.
- Chen, S., Ge, C., Tong, Z., Wang, J., Song, Y., Wang, J., Luo, P., 2022. Adaptformer: Adapting vision transformers for scalable visual recognition. *Advances in Neural Information Processing Systems* 35, 16664–16678.
- Chen, T., Kornblith, S., Norouzi, M., Hinton, G., 2020. A simple framework for contrastive learning of visual representations, in: *International conference on machine learning*, PMLR. pp. 1597–1607.
- Degerli, A., Kiranyaz, S., Chowdhury, M.E., Gabbouj, M., 2022. Osegnet: Operational segmentation network for covid-19 detection using chest x-ray images, in: *2022 IEEE International Conference on Image Processing (ICIP)*, IEEE. pp. 2306–2310.
- Devlin, J., Chang, M.W., Lee, K., Toutanova, K., 2019. Bert: Pre-training of deep bidirectional transformers for language understanding, in: *Proceedings of the 2019 conference of the North American chapter of the association for computational linguistics: human language technologies, volume 1 (long and short papers)*, pp. 4171–4186.
- Dosovitskiy, A., Beyer, L., Kolesnikov, A., Weissenborn, D., Zhai, X., Unterthiner, T., Dehghani, M., Minderer, M., Heigold, G., Gelly, S., et al., 2020. An image is worth 16x16 words: Transformers for image recognition at scale. *arXiv preprint arXiv:2010.11929*.
- Dutt, R., Ericsson, L., Sanchez, P., Tsaftaris, S.A., Hospedales, T., 2024. Parameter-efficient fine-tuning for medical image analysis: The missed opportunity, in: *Medical Imaging with Deep Learning*, PMLR. pp. 406–425.
- Frankle, J., Schwab, D.J., Morcos, A.S., 2020. Training batchnorm and only batchnorm: On the expressive power of random features in cnns. *arXiv preprint arXiv:2003.00152*.
- Fu, M., Zhu, K., Wu, J., 2024. Dtl: Disentangled transfer learning for visual recognition, in: *Proceedings of the AAAI Conference on Artificial Intelligence*, pp. 12082–12090.
- Goodfellow, I., Pouget-Abadie, J., Mirza, M., Xu, B., Warde-Farley, D., Ozair, S., Courville, A., Bengio, Y., 2020. Generative adversarial networks. *Communications of the ACM* 63, 139–144.
- Greenspan, H., Van Ginneken, B., Summers, R.M., 2016. Guest editorial deep learning in medical imaging: Overview and future promise of an exciting new technique. *IEEE transactions on medical imaging* 35, 1153–1159.
- He, A., Wu, Y., Wang, Z., Li, T., Fu, H., 2025. Dvpt: Dynamic visual prompt tuning of large pre-trained models for medical image analysis. *Neural Networks* 185, 107168.
- He, K., Chen, X., Xie, S., Li, Y., Dollár, P., Girshick, R., 2022. Masked autoencoders are scalable vision learners, in: *Proceedings of the IEEE/CVF conference on computer vision and pattern recognition*, pp. 16000–16009.
- He, K., Fan, H., Wu, Y., Xie, S., Girshick, R., 2020. Momentum contrast for unsupervised visual representation learning, in: *Proceedings of the IEEE/CVF conference on computer vision and pattern recognition*, pp. 9729–9738.
- Heller, N., Sathianathan, N., Kalapara, A., Walczak, E., Moore, K., Kaluzniak, H., Rosenberg, J., Blake, P., Rengel, Z., Oestreich, M., et al., 2019. The kits19 challenge data: 300 kidney tumor cases with clinical context, ct semantic segmentations, and surgical outcomes. *arXiv preprint arXiv:1904.00445*.
- Houlsby, N., Giurgiu, A., Jastrzebski, S., Morrone, B., De Laroussilhe, Q., Gesmundo, A., Attariyan, M., Gelly, S., 2019. Parameter-efficient transfer learning for nlp, in: *International conference on machine learning*, PMLR. pp. 2790–2799.
- Hu, E.J., Shen, Y., Wallis, P., Allen-Zhu, Z., Li, Y., Wang, S., Wang, L., Chen, W., et al., 2022. Lora: Low-rank adaptation of large language models. *ICLR* 1, 3.
- Huang, Y., Cheng, P., Tam, R., Tang, X., 2024. Fpt: Fine-grained prompt tuning for parameter and memory efficient fine tuning in high-resolution medical image classification. *arXiv preprint arXiv:2403.07576*.
- Huang, Z., Wang, H., Deng, Z., Ye, J., Su, Y., Sun, H., He, J., Gu, Y., Gu, L., Zhang, S., et al., 2023. Stu-net: Scalable and transferable medical image segmentation models empowered by large-scale supervised pre-training. *arXiv preprint arXiv:2304.06716*.
- Jia, M., Tang, L., Chen, B.C., Cardie, C., Belongie, S., Hariharan, B., Lim, S.N., 2022. Visual prompt tuning, in: *European Conference on Computer Vision*, Springer. pp. 709–727.
- Kang, M., Song, H., Park, S., Yoo, D., Pereira, S., 2023. Benchmarking self-supervised learning on diverse pathology datasets, in: *Proceedings of the IEEE/CVF Conference on Computer Vision and Pattern Recognition*, pp. 3344–3354.

- Kermany, D., Zhang, K., Goldbaum, M., et al., 2018. Labeled optical coherence tomography (oct) and chest x-ray images for classification. *Mendeley data* 2, 651.
- Li, X.L., Liang, P., 2021. Prefix-tuning: Optimizing continuous prompts for generation. *arXiv preprint arXiv:2101.00190* .
- Lian, D., Zhou, D., Feng, J., Wang, X., 2022. Scaling & shifting your features: A new baseline for efficient model tuning. *Advances in Neural Information Processing Systems* 35, 109–123.
- Liao, B., Tan, S., Monz, C., 2024. Make pre-trained model reversible: From parameter to memory efficient fine-tuning. *Advances in Neural Information Processing Systems* 36.
- Liu, W., Shen, X., Pun, C.M., Cun, X., 2023. Explicit visual prompting for low-level structure segmentations, in: *Proceedings of the IEEE/CVF Conference on Computer Vision and Pattern Recognition*, pp. 19434–19445.
- Michelucci, U., 2022. An introduction to autoencoders. *arXiv preprint arXiv:2201.03898* .
- Pan, R., Liu, X., Diao, S., Pi, R., Zhang, J., Han, C., Zhang, T., 2025. Lisa: layerwise importance sampling for memory-efficient large language model fine-tuning. *Advances in Neural Information Processing Systems* 37, 57018–57049.
- Siméoni, O., Puy, G., Vo, H.V., Roburin, S., Gidaris, S., Bursuc, A., Pérez, P., Marlet, R., Ponce, J., 2021. Localizing objects with self-supervised transformers and no labels, in: *BMVC 2021-32nd British Machine Vision Conference*.
- Sirinukunwattana, K., Pluim, J.P., Chen, H., Qi, X., Heng, P.A., Guo, Y.B., Wang, L.Y., Matuszewski, B.J., Bruni, E., Sanchez, U., et al., 2017. Gland segmentation in colon histology images: The glas challenge contest. *Medical image analysis* 35, 489–502.
- Song, Z., Yang, K., Guan, N., Zhu, J., Qiao, P., Hu, Q., 2023. Pvp: Pre-trained visual parameter-efficient tuning. *arXiv preprint arXiv:2304.13639* .
- Su, Y., Wang, X., Qin, Y., Chan, C.M., Lin, Y., Wang, H., Wen, K., Liu, Z., Li, P., Li, J., et al., 2022. On transferability of prompt tuning for natural language processing, in: *Proceedings of the 2022 Conference of the North American Chapter of the Association for Computational Linguistics: Human Language Technologies*, pp. 3949–3969.
- Subramanian, M., Shanmugavadeivel, K., Naren, O.S., Premkumar, K., Rankish, K., 2022. Classification of retinal oct images using deep learning, in: *2022 international conference on computer communication and informatics (ICCCI)*, IEEE. pp. 1–7.
- Sung, Y.L., Cho, J., Bansal, M., 2022. Lst: Ladder side-tuning for parameter and memory efficient transfer learning. *Advances in Neural Information Processing Systems* 35, 12991–13005.
- Tang, N., Fu, M., Zhu, K., Wu, J., 2024. Low-rank attention side-tuning for parameter-efficient fine-tuning. *arXiv preprint arXiv:2402.04009* .
- Touvron, H., Cord, M., El-Nouby, A., Verbeek, J., Jégou, H., 2022. Three things everyone should know about vision transformers, in: *European Conference on Computer Vision*, Springer. pp. 497–515.
- Vincent, P., Larochelle, H., Bengio, Y., Manzagol, P.A., 2008. Extracting and composing robust features with denoising autoencoders, in: *Proceedings of the 25th international conference on Machine learning*, pp. 1096–1103.
- Wang, W., Shen, J., Chen, C., Jiao, J., Liu, J., Zhang, Y., Song, S., Li, J., 2023. Med-tuning: Parameter-efficient transfer learning with fine-grained feature enhancement for medical volumetric segmentation. *arXiv e-prints* , arXiv–2304.
- Wang, Y., Cheng, L., Fang, C., Zhang, D., Duan, M., Wang, M., 2024. Revisiting the power of prompt for visual tuning, in: *Proceedings of the 41st International Conference on Machine Learning*, pp. 50233–50247.
- Wasserthal, J., Breit, H.C., Meyer, M.T., Pradella, M., Hinck, D., Sauter, A.W., Heye, T., Boll, D.T., Cyriac, J., Yang, S., et al., 2023. Totalsegmentator: robust segmentation of 104 anatomic structures in ct images. *Radiology: Artificial Intelligence* 5, e230024.
- Wei, J., Suriawinata, A., Ren, B., Liu, X., Lisovsky, M., Vaickus, L., Brown, C., Baker, M., Tomita, N., Torresani, L., et al., 2021. A petri dish for histopathology image analysis, in: *Artificial Intelligence in Medicine: 19th International Conference on Artificial Intelligence in Medicine, AIME 2021, Virtual Event, June 15–18, 2021, Proceedings*, Springer. pp. 11–24.
- Willemink, M.J., Koszek, W.A., Hardell, C., Wu, J., Fleischmann, D., Harvey, H., Folio, L.R., Summers, R.M., Rubin, D.L., Lungren, M.P., 2020. Preparing medical imaging data for machine learning. *Radiology* 295, 4–15.
- Wu, Y., Wu, Z., Shi, H., Picker, B., Chong, W., Cai, J., 2023. Coactseg: Learning from heterogeneous data for new multiple sclerosis lesion segmentation, in: *International conference on medical image computing and computer-assisted intervention*, Springer. pp. 3–13.
- Yang, C., Wu, Z., Zhou, B., Lin, S., 2021. Instance localization for self-supervised detection pretraining, in: *Proceedings of the IEEE/CVF Conference on Computer Vision and Pattern Recognition*, pp. 3987–3996.
- Ye, Y., Xie, Y., Zhang, J., Chen, Z., Wu, Q., Xia, Y., 2024. Continual self-supervised learning: Towards universal multi-modal medical data representation learning, in: *Proceedings of the IEEE/CVF Conference on Computer Vision and Pattern Recognition*, pp. 11114–11124.
- Ye, Y., Zhang, J., Chen, Z., Xia, Y., 2022. Desd: Self-supervised learning with deep self-distillation for 3d medical image segmentation, in: *International Conference on Medical Image Computing and Computer-Assisted Intervention*, Springer. pp. 545–555.
- Yin, D., Han, X., Li, B., Feng, H., Bai, J., 2024. Parameter-efficient is not sufficient: Exploring parameter, memory, and time efficient adapter tuning for dense predictions, in: *Proceedings of the 32nd ACM International Conference on Multimedia*, pp. 1398–1406.
- Yoo, S., Kim, E., Jung, D., Lee, J., Yoon, S., 2023. Improving visual prompt tuning for self-supervised vision transformers, in: *International Conference on Machine Learning*, PMLR. pp. 40075–40092.
- Zaken, E.B., Goldberg, Y., Ravfogel, S., 2022. Bitfit: Simple parameter-efficient fine-tuning for transformer-based masked language-models, in: *Proceedings of the 60th Annual Meeting of the Association for Computational Linguistics (Volume 2: Short Papers)*, pp. 1–9.
- Zhang, Q., Chen, M., Bukharin, A., He, P., Cheng, Y., Chen, W., Zhao, T., 2023. Adaptive budget allocation for parameter-efficient fine-tuning, in: *11th International Conference on Learning Representations*, ICLR 2023.
- Zhong, Z., Tang, Z., He, T., Fang, H., Yuan, C., 2024. Convolution meets lora: Parameter efficient finetuning for segment anything model. *arXiv preprint arXiv:2401.17868* .
- Zhou, H.Y., Lu, C., Yang, S., Han, X., Yu, Y., 2021. Preservational learning improves self-supervised medical image models by reconstructing diverse contexts, in: *Proceedings of the IEEE/CVF International Conference on Computer Vision*, pp. 3499–3509.
- Zhou, Z., Siddiquee, M.M.R., Tajbakhsh, N., Liang, J., 2019. Unet++: Redesigning skip connections to exploit multiscale features in image segmentation. *IEEE transactions on medical imaging* 39, 1856–1867.